AJAE

Open Access

Vol. 14, No. 3, pp. 263-279, September 2020
doi: https://doi.org/10.5572/ajae.2020.14.3.263
ISSN (Online) 2287-1160, ISSN (Print) 1976-6912

Research Article

Impact Comparison of Synoptic Meteorology and Nationwide/local Emissions on the Seoul Metropolitan Area during High PM Multi-event and Non-event Days

Il-Soo Park[1)], Moon-Soo Park[1),5),*], Yu Woon Jang[2)], Hyeon-Kook Kim[3)], Chang-Keun Song[3)], Jeffrey S. Owen[2)], Sang-Heon Kim[1),6)], Chang-Rae Cho[1)], Cheol-Hee Kim[4)]

[1)]Research Center for Atmospheric Environment, Hankuk University of Foreign Studies, Yongin, Republic of Korea
[2)]Department of Environmental Sciences, Hankuk University of Foreign Studies, Yongin, Republic of Korea
[3)]School of Urban and Environmental Engineering, Ulsan National Institute of Science and Technology, Ulsan, Republic of Korea
[4)]Department of Atmospheric Sciences, Pusan National University, Busan, Republic of Korea
[5)]Department of Climate and Environment, Sejong University, Seoul, Republic of Korea
[6)]Climate Change & Environment Research Center, Sejong University, Seoul, Republic of Korea

***Corresponding author.**
Tel: +82-2-6935-2558
Fax: 82-2-3408-4354
E-mail: moonsoo@sejong.ac.kr

Received: 17 March 2020
Revised: 27 May 2020
Accepted: 26 June 2020

ABSTRACT Meteorology and emissions play very important roles in the concentrations of air pollutants during severe haze/smog periods. This study compares the impacts of synoptic meteorology and nationwide/local emissions during high PM_{10} multi-event and non-event days in the Seoul Metropolitan Area (SMA). The multi-event and non-event cases were selected based on daily mean PM_{10} concentrations in Seoul from January 2014 to March 2019. The multi-event cases in spring and winter were closely associated with weak synoptic winds, while that in autumn was due to the strong winds at the rear side of a strong cold front, which induced the Asian dust event in northeastern China and Korea. The multi-event case in spring was found to be mainly due to series of migratory anticyclones, while winter case was due to the stagnant system after northerly winds. The surrounding low pressure systems as well as high pressure systems could be important to determine whether the synoptic systems would be stagnant or not. The fractional contributions of SMA emissions to the mean PM_{10} and $PM_{2.5}$ concentrations were 24%–35% and 22%–35% for the multi-event cases, respectively. The contributions to the maximum PM_{10} and $PM_{2.5}$ concentrations were larger than those to the mean concentrations by 16%–23% and 19%–26% for the multi-event cases, respectively.

KEY WORDS Seoul metropolitan area, High PM_{10} multi-event days, Synoptic meteorology, Haze and smog, Nationwide/local emission

1. INTRODUCTION

The Seoul metropolitan area (SMA) is a mega city with a population of 26.1 million (http://kosis.kr) (Kim *et al.*, 2018). Multi-event days with high PM_{10} concentrations in the SMA have been an urgent issue for the South Korean society (Park, 2014; Jo and Kim, 2013). In 2019, the Korean government established "The National Council on Climate and Air Quality", a presidential-level agency, with a focus on reducing PM concentrations as well as building international cooperation and domestic strategies.

The mechanisms causing multi-event days in the SMA are complex because the

air quality in this area is impacted by both local emissions and long-range transboundary transport of air pollutants (Seo *et al.*, 2017; Jo and Kim, 2013; Kim *et al.*, 2012; Park *et al.*, 2005). Further knowledge of both local emissions and long-range transboundary processes is needed to develop effective emission mitigation strategies in the SMA as well as throughout Korea (Park *et al.*, 2019, 2018; Park, 2016). The dominant emission source of PM_{10} and NO_2 in the SMA is diesel-powered vehicles (Koo *et al.*, 2008). During the last two decades, there were some studies on the domestic or foreign contributions to the high PM concentration in Korea. Foreign contributions were reported to have ranges from about 30% to about 70% depending on cases and periods (NIER, 2017; Park *et al.*, 2015). According to "The Expert Meeting for Long-range Transboundary Air Pollutants in Northeast Asia" report, the contributions of China emissions to sulfur and nitrate deposition in Korea were 43% and 45% in January and March 2002, respectively (NIER, 2006). The contribution of foreign or China emission to PM concentration in Korea exhibited larger difference among researchers due to the difference of model, analyzed period, and methodologies. The Korea-US Air Quality (KORUS-AQ) campaign showed that China contributed 34% to $PM_{2.5}$ concentrations from 2 May to 12 June 2016 (NIER, 2017), and 68% during May to June 2016 (Choi *et al.*, 2019). According to the summary report of the 4th stage LTP project, China's contribution to major cities in Korea was 32% in 2017. But, the foreign contribution (including China, North Korea, Mongolia) on PM_{10} concentration in Korea was reported to reach 60% yearly (Kim *et al.*, 2017), 66% (Daejeon city) in February 2014 (Jung *et al.*, 2019), 40–65% during 2010–2017 (Bae *et al.*, 2020).

According to the previous studies on high PM_{10} concentration events in Korea, meteorological conditions contributed to high PM_{10} concentration more than emissions (Park *et al.*, 2019; Seo *et al.*, 2018, 2017; Park, 2014). For example, higher PM_{10} concentration events in the SMA frequently occurred on warmer days (Park *et al.*, 2019; Park, 2014). Moreover, during the high PM_{10} concentrations in spring, the SMA was usually governed by local circulation systems under weak synoptic winds (Park *et al.*, 2019). There was no clear criteria to classify weak and strong synoptic winds. And the criteria can be dependent on the location. Conventionally, the synoptic winds were classified as weak when the wind speed at 850 hPa is less than about 5 m s^{-1} (Park, 1994). Sometimes, the Korean Peninsula was influenced by warm and stagnant high-pressure systems (Park *et al.*, 2019; Seo *et al.*, 2018, 2017; Park, 2016). Some simulation studies had suggested that severe $PM_{2.5}$ episodes were driven by stable synoptic weather conditions rather than an abrupt increase in emissions (Kim *et al.*, 2017; Li *et al.*, 2016). Besides the synoptic meteorology and local circulation, vertical distributions of meteorological and/or turbulent parameters in the atmospheric boundary layer could also lead to high PM_{10} concentrations (Li *et al.*, 2018; Pahlow *et al.*, 2005; Zhou *et al.*, 2005). Day-to-day PM_{10} concentrations in Belgium depended more on meteorology than on anthropogenic emissions (Hooyberghs *et al.*, 2005). Nonetheless, high PM_{10} concentration cases tended to be difficult to categorize by their meteorological features in advance. There were many uncertainties and complexities in the meteorological mechanism affecting high PM_{10} concentrations. Moreover, there have not been many studies on the multi-day high PM concentration events.

The main objective of this study was to compare the synoptic meteorological characteristics between the high PM_{10} multi-event days and the non-event days in the SMA. The fractional contributions of the SMA emission to the $PM_{10}/PM_{2.5}$ concentrations were quantified for the multi-event and non-event cases by using The Air Pollution Model (TAPM).

2. DATA AND METHODS

To select the multi-event case, hourly mean PM_{10}, $PM_{2.5}$, SO_2, and NO_2 concentrations, monitored at the Seoul Station from 1 January 2014 to 31 March 2019 ($PM_{2.5}$ data were not available in 2014), were used (http://www.airkorea.or.kr; Fig. 1). The Seoul Station is located at the center of Seoul and is surrounded by many line and area emission sources (Fig. 1). Surface meteorological variables such as wind speed and direction, temperature, and global solar radiation were obtained from the Songwol Station (Seoul Automatic Synoptic Observation Station; https://data.kma.go.kr; Fig. 1). The Songwol Station is located 1.2 km northwest of the City Hall.

When the daily mean PM_{10} concentration in the Seoul Station was greater than the air quality standard for PM_{10} concentration in Korea, 100 μg m^{-3}, the day was classified as a high PM_{10} event day (Park *et al.*, 2019).

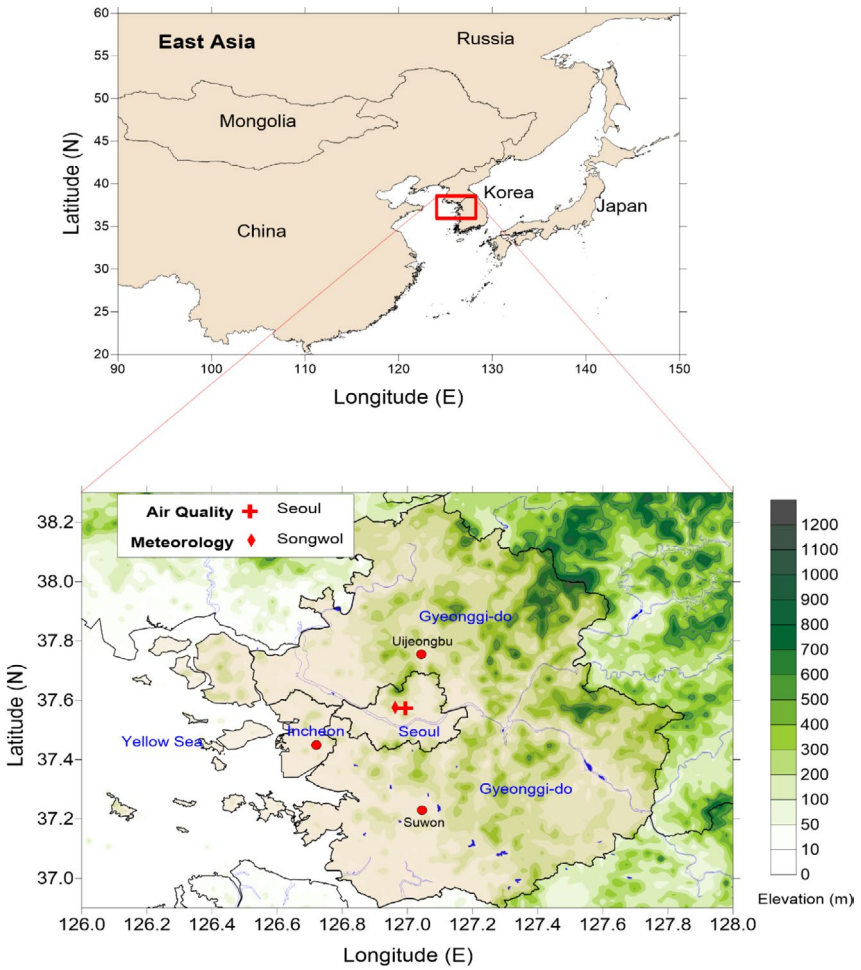

Fig. 1. The innermost model domain and location of air quality monitoring (Seoul Station, cross), and surface meteorological observation (Songwol Station, diamond) stations, Suwon, Incheon and Uijeongbu cities (red circle) used in the study area.

The 7 days, including 5 consecutive event days in spring and winter and 2 consecutive event days in autumn, were classified as multi-day event cases (hereafter, multi-event cases). Korea had no high PM_{10} event days in summer and not so many event days in autumn due to the seasonal dependency of prevailing winds and energy usage with respect to temperature in East Asia. When the daily mean PM_{10} concentration was below 50 $\mu g\,m^{-3}$, the day was classified as a non-event day. The non-event case was chosen as the case of 7 consecutive non-event days in the same month with a multi-event case (Park *et al.*, 2019).

To simulate the 3-dimensional fields of meteorological and air quality concentrations, TAPM was used. TAPM is composed of two prognostic subsections: meteorological and chemical modules (Hurley, 2008). It was set to have three domains with horizontal resolutions of 12 km, 4 km, and 2 km. Each domain had the same number of grid (100 × 100 × 25) with the same center (37°33.97′N, 126°58.67′E). Domain 1 includes South and North Korea, while Domain 3 includes SMA (Seoul, Incheon, and Gyeonggi Province). The Global Assimilation and Prediction System (GASP) data with a resolution at the equator of 0.75° (ftp://ftp.csiro.au/TAPM) were used for the initial boundary field of meteorology (Schulz *et al.*, 2007). It is a spectral model run operationally at every 6 hours by Australia Bureau of Meteorology Research Center. Observation data are assimilated by a generalized statistical interpolation scheme (Steinle, 2005) using an iterative solution similar to that described by (Cohn *et al.*, 1998). Land-use and land-cover data (1 km × 1 km) from the USGS (United States Geological Survey) were used as input parameters.

Table 1. The median concentration of observed PM_{10}, $PM_{2.5}$, NO_2, and SO_2 in the SMA for the multi-event and non-event cases.

Case	Season	Date	PM_{10} ($\mu g\,m^{-3}$)	$PM_{2.5}$ ($\mu g\,m^{-3}$)	NO_2 (ppb)	SO_2 (ppb)
Multi-Event	Spring	28 Feb–6 Mar 2019	113	77	50	5
	Autumn	24–30 Nov 2018	61.5	26	41	4
	Winter	22–28 Feb 2014	126.5	–	56	11
Non-event	Spring	8–14 Mar 2019	46	25	36.5	4
	Autumn	14–20 Nov 2018	40	22	38	4
	Winter	12–18 Feb 2014	27	–	39	5

Table 2. The ratio of mean concentration to the monthly mean concentration of PM_{10}, $PM_{2.5}$, NO_2, and SO_2 in the SMA for the multi-event and non-event cases.

Case	Season	PM_{10} ($\mu g\,m^{-3}$)	$PM_{2.5}$ ($\mu g\,m^{-3}$)	NO_2 (ppb)	SO_2 (ppb)
Multi-Event	Spring	1.94	2.09	1.37	1.27
	Autumn	1.41	1.07	1.04	1.02
	Winter	2.19	–	1.44	1.61
Non-event	Spring	0.78	0.70	1.04	1.02
	Autumn	0.83	0.90	0.98	1.01
	Winter	0.63	–	0.98	–

Fig. 2 illustrates the spatial distribution of total nationwide emissions in 2015 (reference year) of PM_{10}, NO_x, and SO_2 with a resolution of $4 \times 4\,km^2$. Nationwide emissions imply emission rates from all South Korean boundary, while SMA emissions mean emission rates from Seoul City, Incheon City, and Gyeonggi Province. Emission rates were 232,794 ton y^{-1}, 1,000,064 ton y^{-1}, and 351,010 ton y^{-1} nationwide, and 44,385 ton y^{-1}, 289,431 ton y^{-1}, and 37,223 ton y^{-1} in the SMA for PM_{10}, NO_x, and SO_2, respectively (Park *et al.*, 2019). The SMA emissions account for 19.1%, 28.9%, and 10.6% of nationwide emissions for PM_{10}, NO_x, and SO_2, respectively. Emission rates of PM_{10} and NO_x were highly dependent on traffic densities (Park *et al.*, 2019; Park, 2014). Note that emission rates from outside South Korea (such as China, North Korea, and Japan) were not considered in this study. Instead, initial and background concentration and emission rates from South Korea were used to simulate the air pollutant concentrations.

3. AIR POLLUTANTS CONCENTRATION

According to the above criteria, the multi-event and non-event cases were chosen as the periods from 28 February to 6 March and from 8 to 14 March 2019 in spring, from 24 to 30 and from 14 to 20 November 2018 in autumn, and from 22 to 28 and from 12 to 18 February 2014 in winter, respectively (Table 1). The chosen multi-event cases in spring and winter included 6-consecutive high PM_{10} event days from 1 to 6 March 2019 and from 23 to 28 February 2014, respectively. Only 2 cases with 3 or more consecutive event days were found from 2014 to 2019. Fig. 3 shows the time series of PM_{10}, $PM_{2.5}$, NO_2, and SO_2 concentrations for 7 days (from 2 days before to 4 days after the peak value) for multi-event and non-event cases. PM_{10} and $PM_{2.5}$ concentrations throughout the event period were much higher than those throughout the non-event period, except in autumn (Fig. 3). High PM concentration in autumn was due to Asian dust, not smog/haze. There were not so many differences between the multi-event and non-event cases for NO_2 and SO_2, except for SO_2 in winter.

Median concentrations of PM_{10}, $PM_{2.5}$, NO_2, and SO_2 at Seoul station during 7 days for the event and non-event cases were calculated. The median of PM_{10} concentration exhibited its highest value (126.5 $\mu g\,m^{-3}$) in winter and its lowest value (61.5 $\mu g\,m^{-3}$) in autumn for

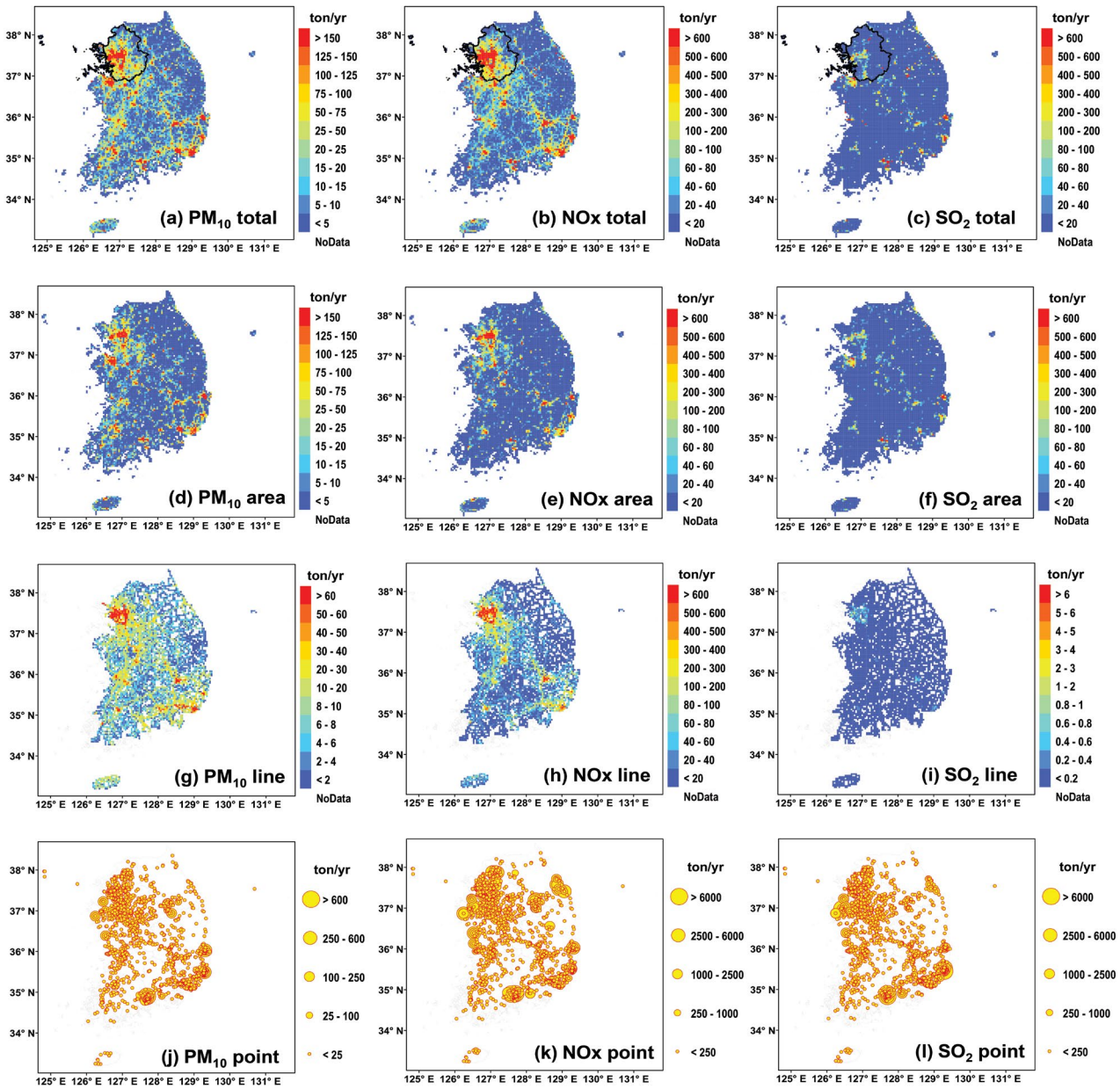

Fig. 2. Total emissions per $4 \times 4\,km^2$ grid of (a) PM_{10}, (b) NO_x, and (c) SO_2; area source emissions of (d) PM_{10}, (e) NO_x, and (f) SO_2; line source emissions of (g) PM_{10}, (h) NO_x, and (i) SO_2; point source emissions of (j) PM_{10}, (k) NO_x, and (l) SO_2 nationwide. Black dotted-lines in the figures (a)–(c) denote the Seoul Metropolitan Area.

the multi-event case, while for the non-event case its highest value ($46\,\mu g\,m^{-3}$) was exhibited in spring and its lowest value ($27\,\mu g\,m^{-3}$) in winter (Table 1). As a result, the PM_{10} concentration ratio of the multi-event case to the non-event case was as high as 4.7 in winter and as low as 1.5 in autumn (Table 1).

The ratios of the case mean PM_{10} concentration to monthly mean concentration were 1.9, 1.4 and 2.2 for the multi-event cases, and 0.8, 0.8, and 0.6 for the non-event cases in spring, autumn, and winter, respectively (Table 2).

Because the TAPM did not include the emission from outside South Korea, the initial background concentrations were set as the monthly mean observed ones on the same month for the multi-event and non-event cases (Table 3).

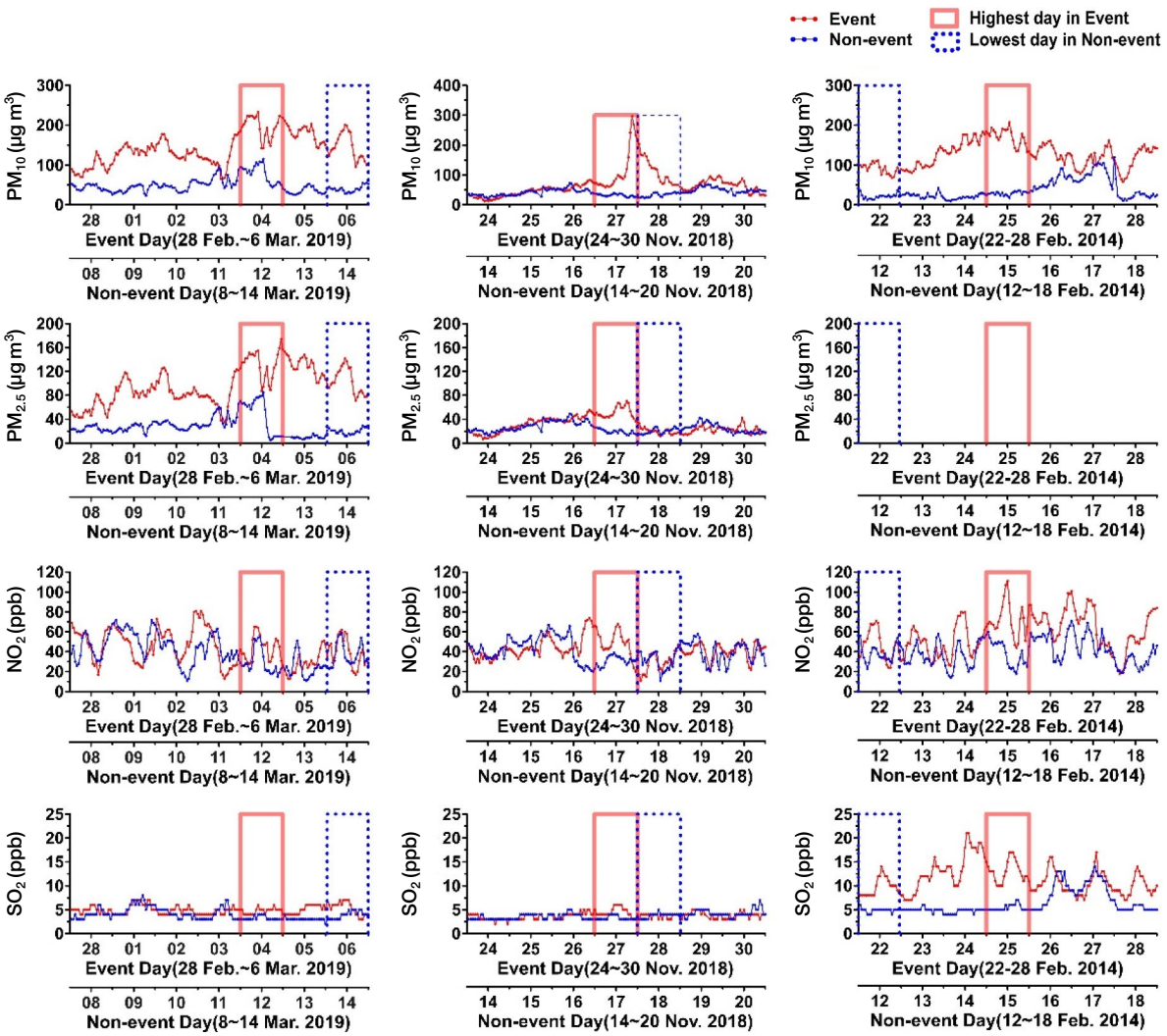

Fig. 3. Time series of PM_{10}, $PM_{2.5}$, NO_2, and SO_2 concentrations in the SMA for the multi-event and non-event cases. The $PM_{2.5}$ data for winter cases in 2014 were not available. Major ticks for x-axis were drawn at 1200 LST on the day.

4. SYNOPTIC METEOROLOGICAL CHARACTERISTICS

Local meteorological factors play an important role in the accumulation of both primary pollutants and secondary aerosol precursors as well as secondary formation processes. They are largely controlled by synoptic-scale conditions (Seo *et al.*, 2017; Zheng *et al.*, 2015). To investigate the synoptic meteorology for the multi-event and non-event cases, surface and upper weather charts were used (http://data.kma.go.kr).

Fig. 4 shows the surface weather chart at 00 UTC during the multi-event (1–6 March 2019) and non-event (9–14 March) cases in spring. During the multi-event case, a weak Siberian high-pressure system and migratory anticyclone systems were located over the Korean Peninsula (Figs. 4a–f). Due to the high-pressure system to the west and low-pressure systems to the east, westerly or northwesterly winds were recorded at the Seoul Station on 28 February and 1 March 2019 (Fig. 4a). Several migratory low-pressure systems generated over southern China or southern Japan on 2–3 March (Figs. 4b, c), evolved, and moved to eastern or northern Japan on 5 March (Fig. 4e). The migratory low-pressure systems to the south or east hindered the weak high-pressure system over Korea from moving eastward, making the system stagnant during 2–5 March 2019 (Figs. 4b–e).

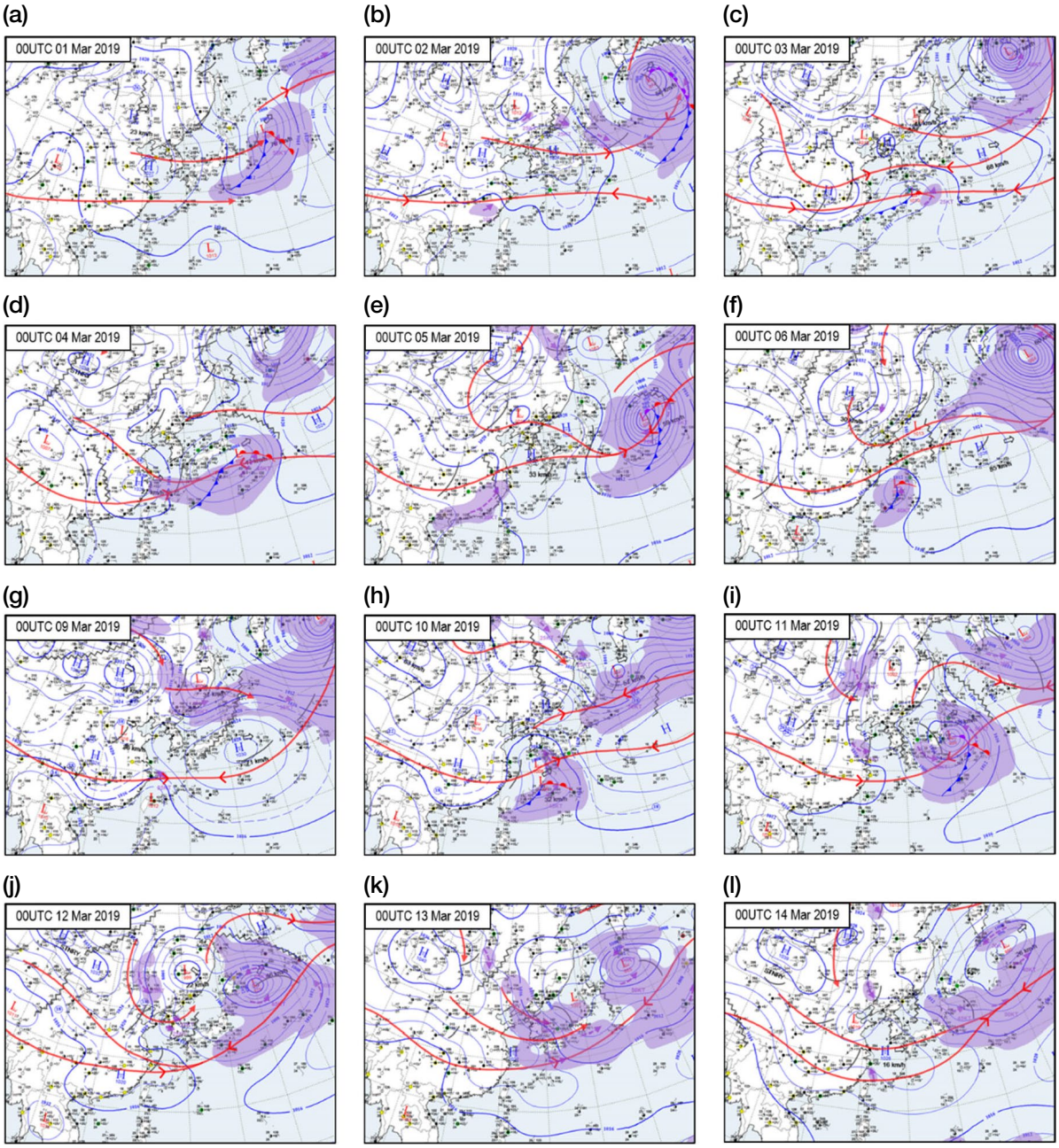

Fig. 4. Surface weather chart at 00 UTC on (a–f) the multi-event days (01–06 March 2019), and (g–l) the non-event days (09–14 March 2019) in spring.

A low-pressure system was centered near eastern Russia, and cloudy conditions were observed over Korea except on 13 March 2019 during the non-event case in spring (Figs. 4g–l). There was little precipitation during 11–14 March. Synoptic systems near the Korean Peninsula can move as fast as 50 km h^{-1}. A low-pressure system, centered over Taiwan on 9 March 2019 (Fig. 4g) evolved, moved to northern Japan on 12 March 2019 (Fig. 4j), and combined with another far eastern-Russia-oriented low-pressure system on 13 March 2019 (Fig. 4k).

The multi-event case on November in 2018 was due to the passage of Asian dust. An array of high-pressure systems extended from southwestern China and moved

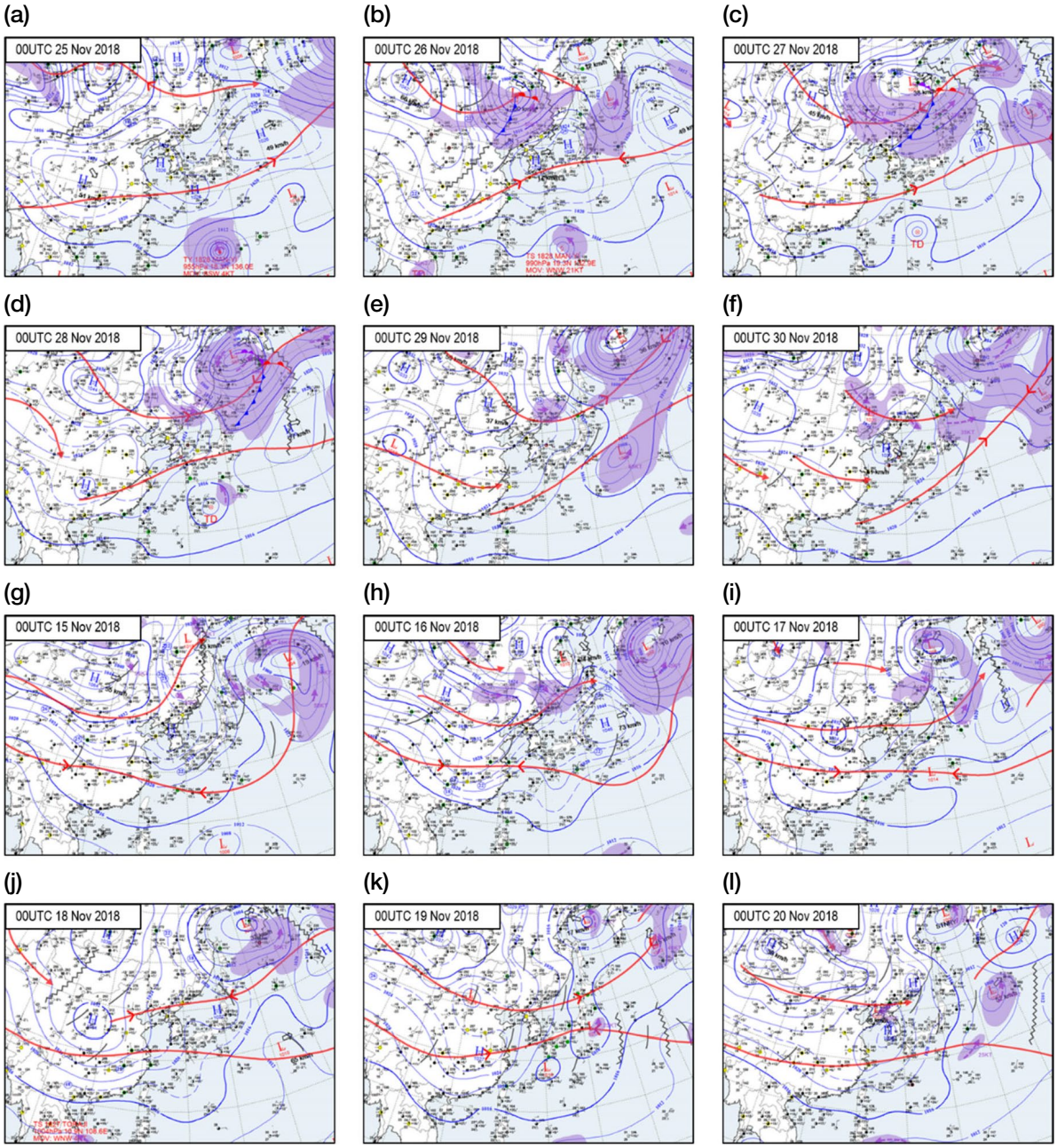

Fig. 5. Surface weather chart at 00 UTC on (a–f) the multi-event days (25–30 November 2018), and (g–l) the non-event days (15–20 November 2018) in autumn.

to eastern Japan on 25 November 2018 during the multi-event case (Figs. 5a–f). A low-pressure system, centered over Lake Baikal on 25 November 2018 (Fig. 5a), moved southeastward. A cold front accompanied by a low-pressure system moved over the Korean peninsula on 26–27 November 2018 (Figs. 5b, c). An Asian dust event, due to the strong wind at the rear side of the cold front, occurred in Seoul on 26–27 November 2018 (Figs. 5b, c).

There was a high-pressure system centered over Mongolia and a low-pressure system located over the Kamchatka peninsula from 15 to 18 November 2018 during the non-event case in autumn (Figs. 5g–j). The high-pressure system extended to the Korean peninsula

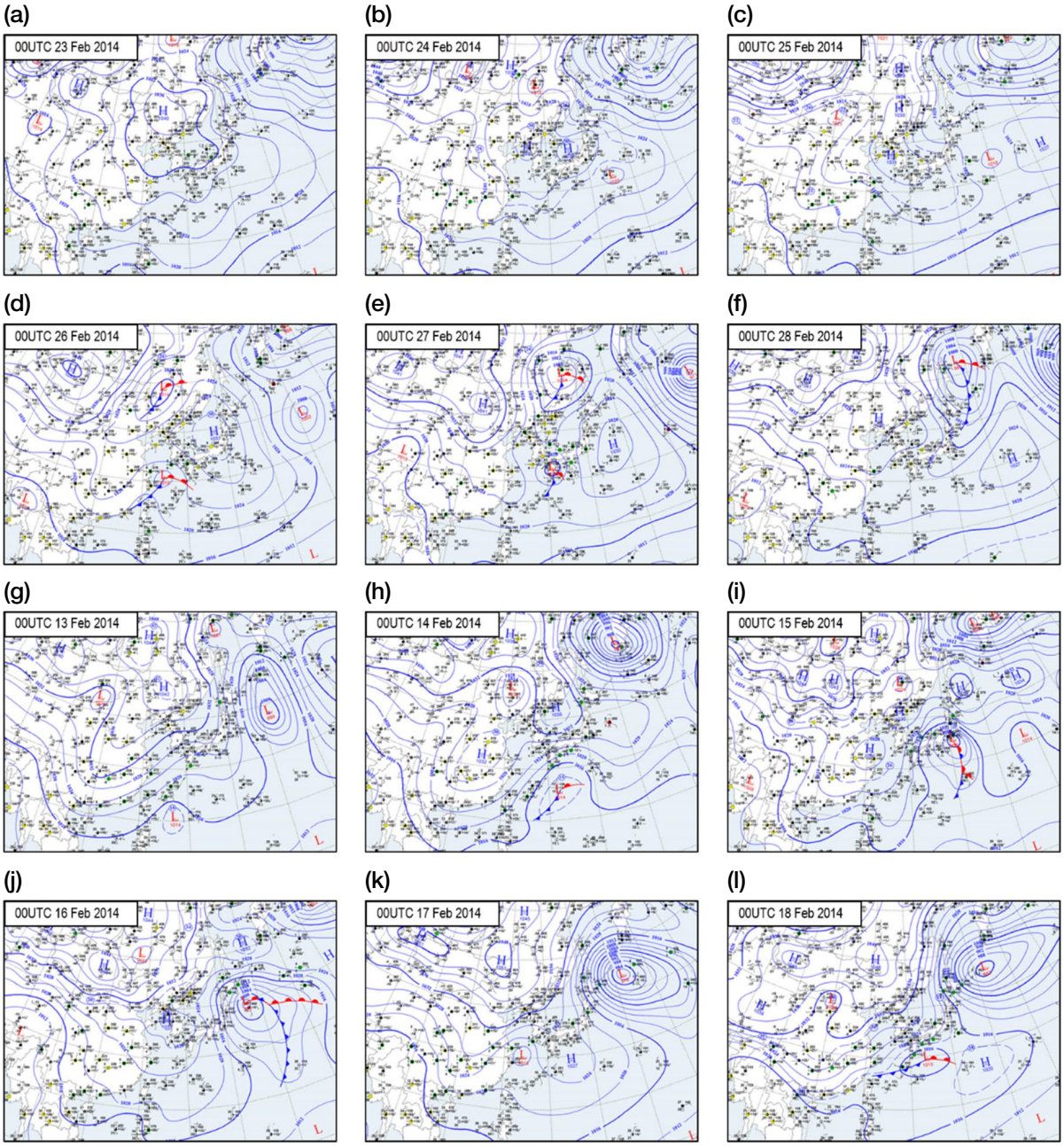

Fig. 6. Surface weather chart at 00 UTC on (a–f) the multi-event days (23–28 Feb 2014) and (g–l) the non-event days (13–18 February 2014) in winter.

and central Japan during this time. Several weak low-pressure systems passed over the Korean peninsula on 19 November 2018 (Fig. 5k). Trace precipitation (0.2 mm) was recorded in Seoul on 20 November 2018 (Fig. 5l).

There was a multi-event case on late February in 2014 (Fig. 6). A migratory anticyclone, centered over northeastern China on 23 February (Fig. 6a), moved to the Korean peninsula on 25 (Fig. 6b), stayed over it during the next two days (Figs. 6c, d), and again moved eastward the next day (Fig. 6e). Two very small and weak low-pressure systems, centered over the northern Korean peninsula and southern Japan, respectively, and passed over the Korean peninsula on 26–27 February

Table 3. Initial background concentrations for TAPM simulation.

Season	PM_{10} ($\mu g\,m^{-3}$)	$PM_{2.5}$ ($\mu g\,m^{-3}$)	NO_2 (ppb)	SO_2 (ppb)	CO (ppm)	O_3 (ppb)
Spring	69	45	33	5	0.6	28
Autumn	47	28	39	5	0.7	11
Winter	57	34	39	6	0.6	16

(Figs. 6c, d).

The boundary between a weak Siberian High-pressure system and a relatively strong low-pressure system, centered between Hokkaido and Kamchatka, was located over Korea throughout the non-event period in winter (Figs. 6g–l). A weak low pressure system with a central pressure of 1013 hPa, centered over eastern Taiwan on 13 February 2014 (Fig. 6g), moved northeastward and reached northern Japan on 17 February (Fig. 6k). The low-pressure system evolved into a strong one with a central pressure of 976 hPa on 17 (Fig. 6k). Due to this high-pressure system over northern Korea and the low-pressure system over southern Korea, easterly winds were recorded in Seoul on 13–14 February 2014 (Figs. 6g, h).

Fig. 7 shows the schematics of synoptic meteorology during the event periods in spring, autumn, and winter. A series of migratory anticyclone systems had formed between two weak cyclone systems located at 30°N and 40°N, and moved into and passed Korean peninsula for spring event case (Fig. 7a). For the autumn event case, a cold front had passed northeastern China on 27 November 2018 (Fig. 7b). Strong winds and Asian dust were accompanied by the cold front. For the winter event case, a high pressure system had moved from northeastern China to Korea, and had been stagnant during two days (Fig. 7c). As a rule, synoptic winds were relatively weak except for autumn Asian dust event case. Stagnant high-pressure or migratory anticyclone systems were dominant near the Korean peninsula for the multi-event cases in spring and winter. The surrounding low pressure systems were also important to determine whether the systems would be stagnant or not. Weak winds and stagnant synoptic systems blocked the horizontal transport of air pollutants, so air pollutants emitted from local sources could accumulate in the atmosphere. Migratory anticyclone systems did continuously transport air pollutants from the source region of China to Korea. On the contrary, for the non-event cases, the winds were not as weak and lower pressure systems were dominant. Strong winds could easily ventilate the polluted air, then made the concentration of air pollutants low.

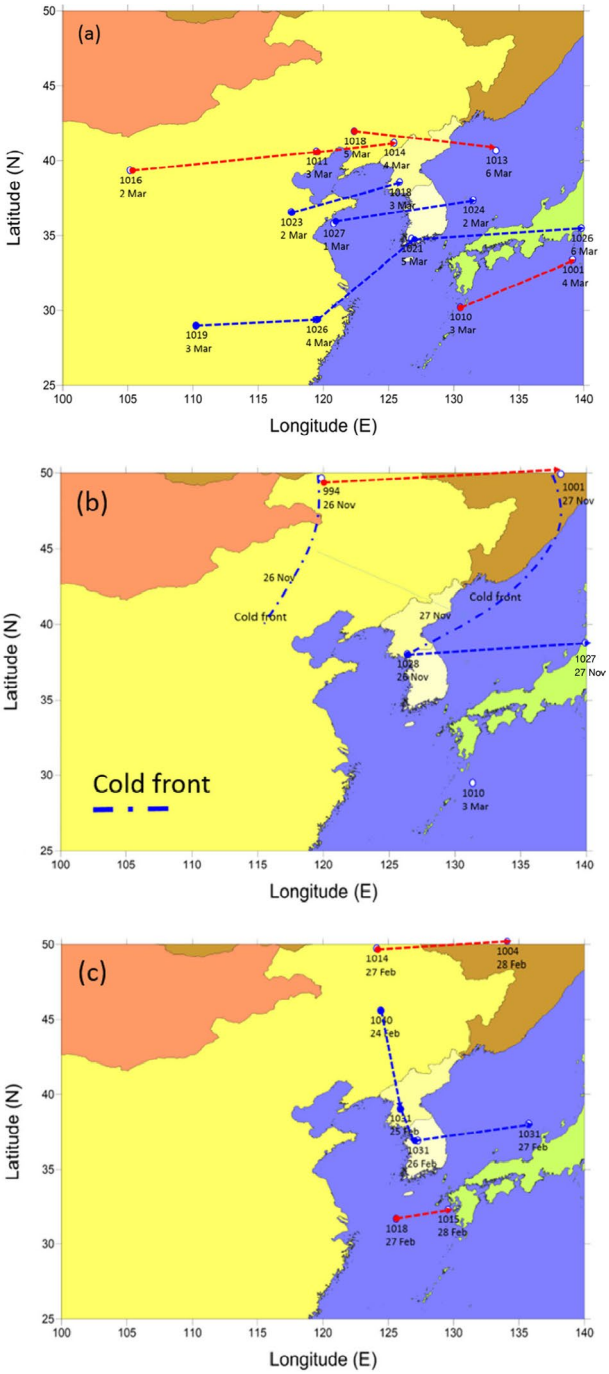

Fig. 7. Location of high and low pressure center with its sea level pressure and moving paths (blue dashed line: high pressure, red dashed line: low pressure) near Korean Peninsula during the event periods in (a) spring, (b) autumn, and (c) winter. Cold fronts are indicated by blue dash dot lines in (b).

Table 4. Mean bias (MB), root mean square error (RMSE), and index of agreement (IOA) between simulated and observed temperature (°C), relative humidity (%), wind speed (m s^{-1}), wind direction (deg), PM_{10} (μg m^{-3}), $PM_{2.5}$ (μg m^{-3}), NO_2 (ppb), and SO_2 (ppb) concentrations for each case.

Case		Meteorology				Concentration			
		Temp	RH	WS	WD	PM_{10}	$PM_{2.5}$	NO_2	SO_2
Spring (Multi-Event)	MB	−1.02	6.3	−0.05	27.1	−37.6	−15.1	12.4	7.9
	RMSE	1.63	14.7	0.88	109.1	61.2	40.1	24.4	10.5
	IOA	0.95	0.88	0.77	0.68	0.24	0.35	0.62	0.58
Spring (Non-event)	MB	−0.74	10.5	0.00	30.9	44.2	27.7	26.6	9.5
	RMSE	1.74	15.1	0.88	130.4	60.5	58.1	33.4	13.4
	IOA	0.93	0.89	0.89	0.57	0.57	0.55	0.64	0.63
Autumn (Multi-Event)	MB	2.16	6.0	0.22	17.4	−6.4	15.8	12.8	6.3
	RMSE	3.14	16.9	0.70	161.7	54.0	30.6	17.1	8.1
	IOA	0.73	0.86	0.73	0.59	−0.11	0.48	0.62	0.59
Autumn (Non-event)	MB	0.25	2.3	0.33	17.1	23.0	21.2	15.3	7.9
	RMSE	1.67	18.6	0.87	153.7	40.8	33.1	22.9	11.0
	IOA	0.92	0.67	0.68	0.65	0.63	0.62	0.62	0.61
Winter (Multi-Event)	MB	0.11	−3.1	−0.63	12.7	−46.4	-	9.3	4.1
	RMSE	1.31	13.4	0.98	117.2	68.5	-	25.0	11.7
	IOA	0.97	0.79	0.68	0.79	0.46	-	0.63	0.67
Winter (Non-event)	MB	−0.73	1.5	−0.49	−12.2	10.9	-	9.48	1.12
	RMSE	1.59	8.4	1.34	105.6	29.7	-	17.4	4.7
	IOA	0.92	0.90	0.26	0.75	0.37	-	0.62	0.68

5. NATIONWIDE/LOCAL EMISSION IMPACT

5.1 Model Evaluation

Fig. 8 shows the time series of temperature, relative humidity, rain, and wind speed and direction observed at the Songwol Station and simulated by TAPM for the multi-event and non-event cases (Fig. 1). Simulated meteorological variables exhibited similar temporal variation with the observed ones, except for the rain. The meteorological variables simulated by TAPM were validated by those observed at the Songwol Station. Statistical performance measures such as the mean bias (MB), root-mean-square error (RMSE), and index of agreement (IOA) were calculated for each case (Table 4). IOA is a frequently used measure of how successful is the simulation of the variable regarding the observed one. The IOA with a value greater than 0.5 is an index of a good simulation (Hurley *et al.*, 2008).

Temperature was underestimated for both cases in spring and the non-event case in winter, while it was overestimated for both cases in autumn. Relative humidity was slightly overestimated except for the multi-event case in winter. Wind was underestimated for both cases in winter. The IOAs for temperature and relative humidity were higher than those for wind speed and direction (Table 4).

The simulated concentrations for PM_{10} and $PM_{2.5}$ show strong diurnal patterns and reveal an underestimation for the multi-event cases and an overestimation for the non-event cases in spring and winter (Fig. 9). It might be mainly related to the same background concentration, which was higher than the mean PM concentration during the non-event case and lower than that during the event case. By and large, the IOAs for $PM_{2.5}$ concentration were larger than those for PM_{10} because TAPM has certain weaknesses in simulating the effect of long-range transported contribution. The simulated NO_2 concentrations were generally in good agreement with the observed ones except for the non-event cases in spring and autumn (Fig. 9). The SO_2 concentration was more or less overestimated for all cases (Fig. 9). This discrepancy seems to be associated mainly with the assumption of constant emissions. The

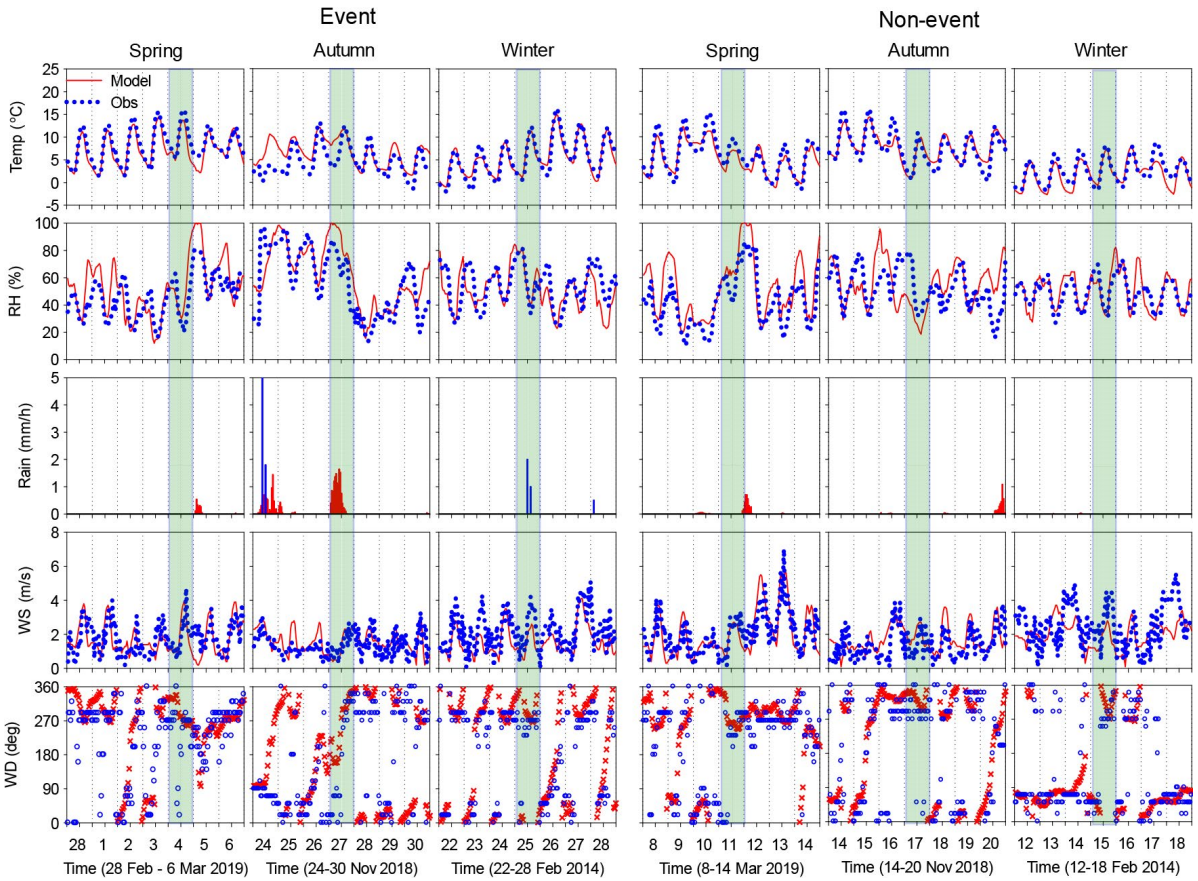

Fig. 8. Time series of temperature (first row), relative humidity (second row), rain (third row), wind speed (fourth row), and wind direction (fifth row) during the event and non-event periods in spring (first, fourth columns), autumn (second, fifth columns), and winter (third, sixth columns), respectively.

IOAs in this study were found to be better than those in recent similar studies in urban areas except those for the multi-event cases in spring and autumn (Park *et al.*, 2018; Hurley *et al.*, 2008).

5.2 Wind and Concentration Fields

Fig. 10 shows the horizontal distribution of PM_{10} with the wind vector simulated with nationwide emissions and without SMA emission for the multi-event and non-event cases. The patterns are strongly governed by the wind; upwind regions showed the lowest concentrations while downwind regions showed the highest concentrations. The areas with the confluent wind exhibited the highest concentrations while the areas with the divergent wind exhibited the lowest concentrations.

In spring, the overall concentration field for nationwide emissions for the multi-event case showed the horizontal distribution with higher concentrations in the central SMA while the highest one was recorded in the western coastal area. The highest concentration might result from the high density of point sources such as power plants, industrial complexes, and steel production facilities near the area. High concentrations in central SMA might be due to the high density of line sources, and somewhat higher PM_{10} concentrations in the northeast might be due to cement manufacturing facilities. For the non-event case, industrial complexes in the southwest were a major contribution to the high PM_{10} concentration in the SMA due to the prevailed westerly wind (Park *et al.*, 2019).

In winter, the PM_{10} concentration for the multi-event days was higher in the southern area due to the prevailing northwesterly wind. Due to strong winds in winter, the overall concentration field showed a homogeneous horizontal distribution pattern except for the high

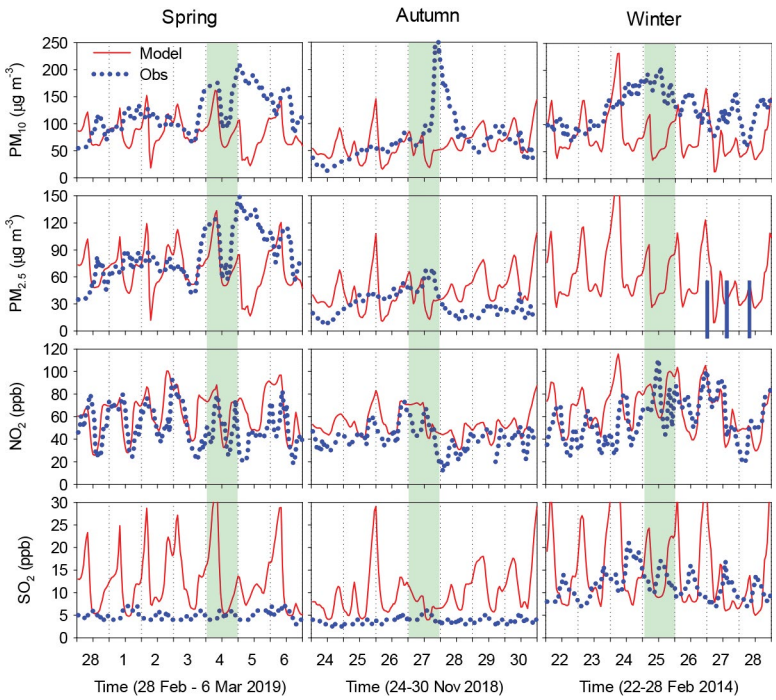

Fig. 9. Time series of PM_{10} (first row), $PM_{2.5}$ (second row), NO_2 (third row), and SO_2 (fourth row) concentrations during the event periods in spring (first columns), autumn (second columns), and winter (third columns), respectively.

PM_{10} concentrations that peaked in the western coastal area and the SMA. It should be noted that point sources including industrial combustion, electric utility, incineration, cement manufacturing, and residential heating facilities in the satellite cities located to the northeast and east of the SMA were important local sources that account for approximately 50 $\mu g\,m^{-3}$ in the SMA. For the non-event case, point sources in the northeast were major contributions to the high PM_{10} concentration in the SMA due to the prevailing northeast wind with the stronger wind (Park *et al.*, 2019).

In autumn, the multi-event case was influenced by an Asian dust storm, and the overall concentration field showed a more homogeneous horizontal distribution except for the high PM_{10} concentrations in the western coastal area. For the non-event case, the overall concentration field was similar to the horizontal distribution for the event days except for the high PM_{10} concentrations in the SMA.

5. 3 Effects of SMA Emissions on the Air Pollutants Concentrations in the SMA

To quantify the effects of SMA emission on the air pollutants concentrations in the SMA for the multi-event and non-event cases, the TAPM model simulated the meteorological variables and air quality concentration with the same initial meteorological field, concentration, and two different modes of emissions for each case (Table 1 and Fig. 2). One mode refers to the nationwide emissions, and the other to the non-SMA emissions (nationwide–SMA). This approach is the same as the Brute-Force Method (BFM) by which we zero-out the emissions in the targeted area (Park *et al.*, 2019; Koo *et al.*, 2008). In order to figure out the effect of local emission on the SMA concentration, the air pollutant concentrations averaged over 4 stations in SMA (Seoul, Incheon, Suwon, and Uijeongbu) were used (Fig. 1). Table 5 shows the mean concentrations in the SMA simulated by nationwide and non-SMA emissions of PM_{10}, $PM_{2.5}$, NO_2, and SO_2 during the multi-event and non-event cases. The difference between mean concentrations and the fractional contribution for each case are listed in Table 5. The fractional contribution was simply calculated by the ratio (%) of concentration simulated with the use of the SMA emission to concentration simulated with the use of the nationwide emission.

For the multi-event cases, the fractional contribution of SMA emissions to the mean PM_{10} concentration was

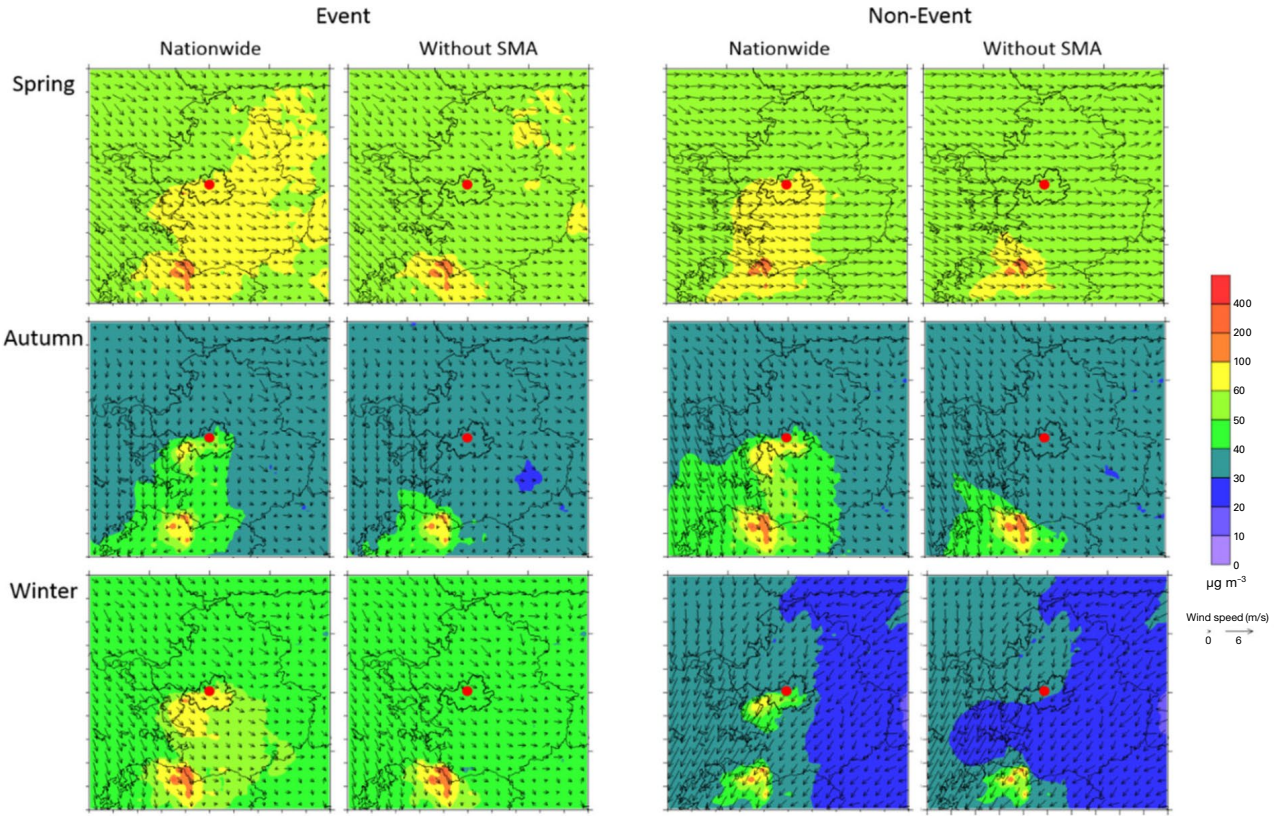

Fig. 10. Horizontal distribution of PM_{10} concentration with wind vector considering nationwide (first and third column) and without SMA (second and fourth column) emissions on event (first and second column) and non-event (third and fourth column) periods in spring (first row), autumn (second row), and winter (third row), respectively. The center of Seoul is indicated by a red circle.

as low as 25% in spring, while as high as 32% in winter. The fractional contribution to the mean $PM_{2.5}$ concentration was similar to or lower than the one to the PM_{10} concentrations. For the non-event cases, the fractional contribution to the mean PM_{10} concentration was similar to, larger than, and lower than those for the multi-event cases in spring, autumn, and winter, respectively. The fractional contribution to the mean NO_2 concentration was as high as 46%–51% for both cases in spring, while as low as 32%–36% for the multi-event case in autumn and the non-event case in winter. High fractional contribution to the NO_2 concentration might be related to the domestic dominant cases rather than long-range transported cases. The fractional contribution to the mean SO_2 concentration was 49%–53%, except for the event case (61%) in winter. These fractional contributions were similar to those in the previous study (Park *et al.*, 2019).

PM_{10} and $PM_{2.5}$ mean concentrations simulated with the use of nationwide and SMA emission for event cases were higher than those for non-event cases, except for autumn. The fractional contributions to the PM_{10} and $PM_{2.5}$ concentrations for event cases were similar to those for non-event cases in all seasons. The concentrations of air pollutants in the SMA were strongly influenced by the outside area of the SMA as well as inside.

6. SUMMARY AND DISCUSSION

The impacts of synoptic meteorology and nationwide/local emissions in the SMA during the high PM_{10} multi-event and non-event days were compared. The multi-event cases were selected among the consecutive high PM_{10} event days with a daily mean concentration $\geq 100\ \mu g\ m^{-3}$ in spring, autumn, and winter. The non-event cases were selected among the consecutive days with a daily mean PM_{10} concentration $< 50\ \mu g\ m^{-3}$ in the same month as the event cases. The cases of 5 consecu-

Table 5. Mean concentration in the SMA simulated by applying the nationwide and non-SMA emissions for the multi-event and non-event cases. Fraction indicates the ratio of the SMA contribution to the nationwide emission in %.

Season			PM_{10} ($\mu g\,m^{-3}$)	$PM_{2.5}$ ($\mu g\,m^{-3}$)	NO_2 (ppb)	SO_2 (ppb)
Spring	Event	Nationwide	73.5	58.4	47.8	8.5
		SMA	55.0	44.4	23.5	4.0
		Reduced Conc.	18.5	14.0	24.3	4.5
		Fraction (%)	25.2	24.0	50.8	52.9
	Non-event	Nationwide	70.8	56.3	47.0	8.7
		SMA	54.0	44.0	25.3	4.3
		Reduced Conc.	16.8	12.3	21.7	4.3
		Fraction (%)	23.7	21.8	46.2	49.4
Autumn	Event	Nationwide	50.0	35.2	44.8	7.1
		SMA	33.5	23.1	30.1	3.6
		Reduced Conc.	16.5	12.1	14.7	3.5
		Fraction (%)	33.0	34.4	32.8	49.3
	Non-event	Nationwide	54.9	38.9	44.3	7.5
		SMA	35.7	24.9	28.4	3.6
		Reduced Conc.	19.2	14.0	15.9	3.9
		Fraction (%)	35.0	36.0	36.0	52.0
Winter	Event	Nationwide	65.0	48.1	49.1	8.9
		SMA	44.1	32.7	28.1	4.6
		Reduced Conc.	20.9	15.4	21.0	4.3
		Fraction (%)	32.2	32.0	42.8	48.3
	Non-event	Nationwide	45.0	33.1	42.5	5.6
		SMA	29.4	21.9	29.0	2.2
		Reduced Conc.	15.6	11.2	13.5	3.4
		Fraction (%)	34.7	33.8	31.8	60.7

tive high PM_{10} event days in spring and winter, and 2 consecutive days in autumn were chosen as the multi-event cases. The high PM concentration of the latter was mainly due to the Asian dust (natural mineral dust) and not the anthropogenic smog and haze.

The synoptic meteorological conditions played an important role in high concentrations. For the multi-event cases in spring and winter, high PM_{10} concentrations were accompanied by weak migratory anticyclone systems over the Korean Peninsula. The horizontal range of surface pressure near the Korean Peninsula was very small, implying that the synoptic system near the SMA was weak and stagnant. On the contrary, synoptic winds for the non-event cases were not so weak as those in the multi-event cases.

The horizontal distribution of meteorological variables and concentration of air pollutants were simulated using the TAPM. The horizontal distributions of concentration were strongly governed by the confluence and divergence of wind as well as upwind or downwind of the major emission sources. To quantify the effects of SMA emissions on the air pollutants' concentration in the SMA, TAPM simulated the same initial background concentration and meteorological boundary condition, and two different scales of emissions (nationwide emissions and non-SMA emissions) for the multi-event and non-event cases. The fractional contribution of SMA emissions to the mean PM_{10} concentrations was as low as 25% in spring, while as high as 33% in autumn and winter for the multi-event cases. The contribution to the mean $PM_{2.5}$ concentration was similar to or lower than those to the mean PM_{10} concentration. Moreover, the contribution to the mean NO_2 (SO_2) concentration was much higher than the one to the mean PM

concentration, except for in autumn.

These contributions for the multi-event cases were much higher than those for the single-event cases in the previous studies. As the high PM concentration period becomes longer, the local emissions contribute more to the formation of high concentrations.

Because the SMA in Korea is surrounded by mountains on three sides, except the west where the Yellow Sea is located, the air quality is influenced by the local circulation such as sea-land breeze and mountain-valley breeze (Park and Chae, 2018; Park, 2018; Oh *et al.*, 2015). This implies that, apart from synoptic meteorology, the vertical structure of meteorological variables in the atmospheric boundary layer can also be an important factor that enhances the concentration of air pollutants. A more detailed analysis of the local circulation and vertical transport is needed to interpret the mechanism of high PM concentrations more accurately, especially in the SMA.

ACKNOWLEDGEMENT

This research was funded by the Korea Meteorological Administration Research and Development Program under Grant KMI2018-05310. Authors would like to thank the NIER (National Institute of Environmental Research) for providing the air quality data, and Prof. Jung-Hun Woo at Konkuk University for providing the Korean emission data by major sectors.

CONFLICTS OF INTEREST

The authors declare no conflict of interest.

REFERENCES

Bae, M., Kim, B.-U., Kim, H.C., Kim, S. (2020) A multiscale tiered approached to quantify contributions: a case study of $PM_{2.5}$ in South Korea during 2010–2017. Atmosphere, 11, 141. https://doi.org/10.3390/atmos11020141

Choi, J., Park, R., Lee, H.-M., Lee, S., Jo, D.S., Jeong, J.I., Henze, D.K., Woo, J.-H., Ban, S.-J., Lee, M.-D., Lim, C.-S., Park, M.-K., Shin, H., Cho, S., Peterson, D., Song, C.-K. (2019) Impacts of local vs. trans-boundary emissions from different sectors on $PM_{2.5}$ exposure in South Korea during the KORUS-AQ campaign. Atmospheric Environment, 203, 196–205. https://doi.org/10.1016/j.atmosenv.2019.02.008

Cohn, S.E., da Silva, A., Guo, J., Sienkiewicz, M., Lamich, D. (1998) Assessing the effects of data selection with the DAO physical-space statistical analysis system. Monthly Weather Review, 126, 2913–2926. https://doi.org/10.1175/1520-0493 (1998)126<2913:ATEODS>2.0.CO;2

Hooyberghs, J., Mensink, C., Dumont, G., Fierens, F., Brasseur, O. (2005) A neural network forecast for daily average PM_{10} concentrations in Belgium. Atmospheric Environment, 39, 3279–3289. https://doi.org/10.1016/j.atmosenv.2015.01.050

Hurley, P.J. (2008) TAPM V4. Part 1: Technical Description, CSIRO Marine and Atmospheric Research Paper, No. 25, 59 pp.

Hurley, P.J., Mary, E., Ashok, L. (2008) TAPM V4. Part 2: Summary of Some Verification Studies. CSIRO Marine and Atmospheric Research Paper, No. 26, 31 pp.

Jo, H.-Y., Kim, C.-H. (2013) Identification of long-range transported haze phenomena and their meteorological features over Northeast Asia. Journal of Applied Meteorology and Climatology, 52, 1318–1328. https://doi.org/10.1175/JAMC-D-11-023.1

Joint Research Project for Long-range Transboundary Air Pollutants in Northeast Asia (2019) Summary Report of the 4th stage (2013–2017) LTP Project. Research Report to National Institute of Environmental Research (Available at http://www.me.go.kr).

Jung, J., Ghim, Y.S., Lyu, Y.S., Lim, Y.-J., Park, J., Sung, M.-Y. (2019) Quantification of regional contributions to fine particles at downwind areas under Asian continental outflows during winter 2014. *Atmospheric Environment*, 210, 231–240. https://doi.org/10.1016/j.atmosenv.2019.04.062

Kim, C.-H., Park, S.-Y., Kim, Y.-J., Chang, L.-S., Song, S.-K., Moon, Y.-S., Song, C.-K. (2012) A numerical study on indicators of long-range transport potential for anthropogenic particulate matters over northeast Asia. Atmospheric Environment, 58, 35–44. https://doi.org/10.1016/j.atmosenv.2011.11.002

Kim, H.C., Kim, E., Bae, C., Cho, J.H., Kim, B.U., Kim, S. (2017) Regional contributions to particulate matter contribution in the Seoul Metropolitan Area, Korea: Seasonal variation and sensitivity to meteorology and emission inventory. Atmospheric Chemistry and Physics, 17, 10315–10332. https://doi.org/10.5194/acp-17-10315-2017

Kim, Y.P., Lee, G., Park, R. (2018) Preface to a special Issue "Megacity Air Pollution Studies (MAPS)". Aerosol and Air Quality Research, 18, I–IV. https://doi.org/10.4209/aaqr.2018.09.maps

Koo, B., Wilson, G.M., Morris, R.E., Dunker, A.M., Yarwood, G. (2009) Comparison of source apportionment and sensitivity analysis in a particulate matter air quality model. Environmental Science and Technology, 43(17), 6669–6675. https://doi.org/10.1021/es9008129

Koo, Y.S., Kim, S.T., Yun, H.Y., Han, J.S., Lee, J.Y., Kim, K.H., Jeon, E.C. (2008) The simulation of aerosol transport over East Asia region. Atmospheric Research, 90, 264–271. https://doi.org/10.1016/j.atmosenv.2008.03.014

Li, S., Ma, Z., Xiong, X., David, C.C., Wang, Z., Liu, Y. (2016)

Satellite and ground observations of severe air pollution episodes in the winter of 2013 in Beijing, China. Aerosol and Air Quality Research, 16, 977–989. https://doi.org/10.4209/aaqr.2015.01.0057

Li, X., Wang, Y., Zhao, H., Hong, Y., Liu, N., Ma, J. (2018) Characteristics of pollutants and boundary layer structure during two haze events in summer and autumn 2014 in Shenyang, Northeast China. Aerosol and Air Quality Research, 18, 386–396, https://doi.org/10.4209/aaqr.2017.03.0100

NIER (National Institute of Environmental Research in Korea). (2006) The 9th Expert Meeting for the L Transboundary Air Pollutants in Northeast Asia, The 9th Working Group Meeting & the 8th Sub-Working Group Meeting, Incheon, South Korea, 473 pp.

NIER (National Institute of Environmental Research in Korea). (2017) Introduction to the KORUS-AQ Rapid Science Synthesis Report, Incheon, South Korea, 35 pp.

Oh, H.-R., Ho, C.-H., Kim, J., Chen, D., Lee, S., Choi, Y.-S., Chang, L.-S., Song, C.-K. (2015) Long-range transport of air pollutants originating in China: A possible major cause of multi-day high-PM_{10} episodes during cold season in Seoul, Korea. Atmospheric Environment, 109, 23–30. https://doi.org/10.1016/j.atmosenv.2015.03.005

Pahlow, M., Kleissl, J., Parlange, M.B. (2005) Atmospheric boundary-layer structure observed during a haze event due to forest-fire smoke. Boundary-Layer Meteorology, 114, 53–70. https://doi.org/10.1007/s10546-004-6350-z

Park, I.-S. (2014) Creative counter-measures of PM_{10}. Journal Korean Society of Atmospheric Environment, 30(2), 211–212.

Park, I.-S. (2016) Why do the high concentration PM_{10} episodes occur and what is the major cause of the episodes? Journal of Korean Society of Atmospheric Environment, 32(3), 352–353.

Park, I.-S., Choi, W.-J., Lee, T.-Y., Lee, S.-J., Han, J.-S., Kim, C.-H. (2005) Simulation of long-range transport of air pollutants over Northeast Asia using a comprehensive acid deposition model. Atmospheric Environment, 39, 4075–4085. https://doi.org/10.1016/j.atmosenv.2005.03.038

Park, I.-S., Song, C.-K., Park, M.-S., Kim, B.-G., Jang, Y. W., Ha, S.-S., Jang, S.-H., Chung, K.-W., Lee, H.-J., Lee, U.-J., Kim, S.-K., Kim, C.-H. (2018) Numerical study on the impact of power plants on primary PM_{10} concentrations in South Korea. Asian Journal of Atmospheric Environment, 12(3), 255–273. https://doi.org/10.5572/ajae.2018.12.3.255

Park, I.-S., Kim, H.-K., Song, C.-K., Jang, Y-W., Kim, S-H., Cho, C-R., Owen, J.S., Kim, C.-H., Chung, K.-W., Park, M.-S. (2019) Meteorological Characteristics and Assessment of the Effect of Local Emissions during High PM_{10} Concentration in the Seoul Metropolitan Area. Asian Journal of Atmospheric Environment, 13(2), 117–135. https://doi.org/10.5572/ajae.2019.13.2.117

Park, M.-S. (2018) Overview of meteorological surface variables and boundary-layer structures in the Seoul Metropolitan Area during the MAPS-Seoul campaign. Aerosol and Air Quality Research, 18, 2157–2172. https://doi.org/10.4209/aaqr.2017.10.0428

Park, M.-S., Chae, J.-H. (2018) Features of sea-land-breeze circulation over the Seoul Metropolitan Area. Geoscience Letters, 5, 28. https://doi.org/10.1186/s40562-018-0127-6

Park, S.-U. (1994) Air quality simulations using surface meteorological observation data. Journal of Korean Meteorological Society, 30(3), 469–486.

Park, S.-U., Lee, I.H., Choe, A., Joo, S.J. (2015) Contributions of the pollutant emission in South Korea to the aerosol concentrations and depositions in Asia. Asia-Pacific Journal of Atmospheric Sciences, 51, 183–195. https://doi.org/10.1007/s13143-015-0069-2

Seo, J., Kim, J.Y., Yoon, D., Lee, J.Y., Kim, H., Lim, Y.B., Kim, Y., Jin, H.C. (2017) On the multiday haze in the Asian continental outflow: the important role of synoptic conditions combined with regional and local sources. Atmospheric Chemistry and Physics 17, 9311–9332. https://doi.org/10.5194/acp-17-9311-2017

Seo, J., Park, D.-S., Kim, J.Y., Youn, D., Lim, Y.B., Kim, Y. (2018) Effects of meteorology and emissions on urban air quality: a quantitative statistical approach to long-term records (1996–2016) in Seoul, South Korea. Atmospheric Chemistry and Physics, 18, 16121–16137, https://doi.org/10.5194/acp-18-16121-2018

Schulz, E.Z., Depert, J.D., Greenslade, D.J. (2007) An assessment of marine surface wind from the Australian Bureau of Meteorology Numerical Weather Prediction System. Wether Forecast, 22, 613–636. https://doi.org/10.1175/WAF996.1

Steinle, P.J. (2005) Generalized statistical interpolation. Fourth Symposium on Assimilation of Observations for Meteorology and Oceanography, Prague, Czech Republic, WMO, CD-ROM.

Zheng, G.J., Duan, F.K., Su, H., Ma, Y.L., Cheng, Y., Zheng, B., Zhang, Q., Huang, T., Kimoto, T., Chang, D., Pöschl, U., Cheng, Y.F., He, K.B. (2015) Exploring the severe winter haze in Beijing: the impact of synoptic weather, regional transport and heterogeneous reactions. Atmospheric Chemistry and Physics, 15, 2969–2983. https://doi.org/10.5194/acp-15-2969-2015

Zhou, L., Xu, X., Ding, G., Zhou, M., Cheng, X. (2005) Diurnal variations of air pollution and atmospheric boundary layer structure in Beijing during winter 2000/2001. Atmospheric Sciences, 22, 126–132. https://doi.org/10.1007/BF02930876